Chemical Engineering Journal 454 (2023) 140431

Contents lists available at ScienceDirect

Chemical Engineering Journal

journal homepage: www.elsevier.com/locate/cej

Modified metal–organic framework by a novel coordinatively unsaturated amine grafting mechanism for direct air capture of CO_2

Fengsheng Liu [a,b], Tao Wang [a,b,*], Hao Dong [a], Weishan Liu [a]

[a] State Key Laboratory of Clean Energy Utilization, Zhejiang University, Hangzhou 310027, China
[b] Key Laboratory of Clean Energy and Carbon Neutrality of Zhejiang Province, Hangzhou 310027, China

ARTICLE INFO

Keywords:
Direct air capture
Amines
MIL-100(Cr)
Adsorption
Desorption

ABSTRACT

This study aimed to improve the carbon dioxide (CO_2) capture and kinetics performance for direct air capture (DAC) while demonstrating the amine grafting reaction principles and its constraints using N-(2-aminoethyl) ethanolamine (AEEA) to functionalize coordinatively unsaturated metal sites in MIL-100(Fe), UiO-66(Zr), and MIL-100(Cr). Grafting experiments indicated that the grafting process is the reaction between metal sites and secondary amines of AEEA, while MOFs with high surface area and low acidity can effectively promote amine grafting without destroying the active site. Moreover, the adsorbed CO_2 amounts of MF-Cr-AEEA at 400 ppm were 1.91 mmol/g of −25 °C and 2.42 mmol/g of 0 °C, and the structural decomposition temperature exceeded 400 °C, demonstrating excellent thermal and cold stability. As a result of the better crystal and surface structure, the internal heat and mass transfer processes were accelerated, resulting in low semi-adsorption times below 21 min. Moreover, CO_2 capture cycles were established at 25 °C for adsorption and 80 °C for desorption. The results show that the adsorption capacity of MF-Cr-AEEA remained 1.86 mmol/g after seven cycles, demonstrating low renewable energy consumption and high stability.

1. Introduction

An exponential increase in global economic development, global trade, and population growth has led to increased carbon dioxide (CO_2) emissions, leading to more frequent natural disasters such as glacier melting, sea-level rise, extreme weather, and ozone depletion [1]. The atmospheric CO_2 concentration exceeds 410 ppm, exceeds 70 % of society's pre-industrial levels, and is forecasted to exceed 550 ppm by 2050 [2]. Therefore, it is imperative that Carbon Capture, Utilization, and Storage (CCUS) technology must be vigorously developed. Among various capture technologies, Direct Air Capture (DAC) as one of the most promising negative emission technologies is a process designed to separate CO_2 from ambient air using a sorption technology [3]. The primary advantages of DAC are its small land requirement, high efficiency of processing dispersed combustion emission sources, and flexibility in terms of CO_2 storage and utilization [3]. However, the ultra-low CO_2 concentration of 400 ppm and the high energy consumption required for regeneration using high-alkaline functional groups (NaOH, or KOH) have limited the development of DAC technology [4].

To solve these problems, several supported-amines adsorbents, such as zeolites [5,6], metal oxide [7,8], activated carbons [9,10], and resin [11,12], are used in air CO_2 capture. The mass transfer barrier and the ideal molecular unit thickness of adsorbents are decreased through physical dispersion, which promotes the binding of amines to material pores. However, because the disordered stack of amines blocks the exposure of active sites, the CO_2 diffusion is slow, further reducing the adsorption capacity [13,14]. Badanicova et al. [13] loaded polyethylenimine (PEI) with Santa Barbara Amorphous-15 (SBA-15) to obtain a supported-amine adsorbent with adsorption performance of only 0.19 mmol/g at 303 K due to blockage of carrier channels. Comparatively, the chemical grafting method can effectively enhance the homogeneity and stability of adsorbents through the reaction of surface functional groups in carrier molecules with amine groups [15,16]. Thus, designing a novel and stable chemical grafting carrier material for efficient adsorption at ultra-low partial pressure is quite critical.

Metal-organic frameworks (MOFs), as a topological structure formed by the self-assembly of metal ions and organic ligands, is potential material for chemical grafting [17,18]. Depending on the choice of ligands and metal ions, MOFs can obtain specified surface morphology with rich Lewis (L) and Brønsted (B) acid sites [4,17]. Due to the large polarizability and quadrupole moment of CO_2, the exposed L acid sites

* Corresponding author.
E-mail address: oatgnaw@zju.edu.cn (T. Wang).

https://doi.org/10.1016/j.cej.2022.140431
Received 15 July 2022; Received in revised form 3 November 2022; Accepted 14 November 2022
Available online 17 November 2022

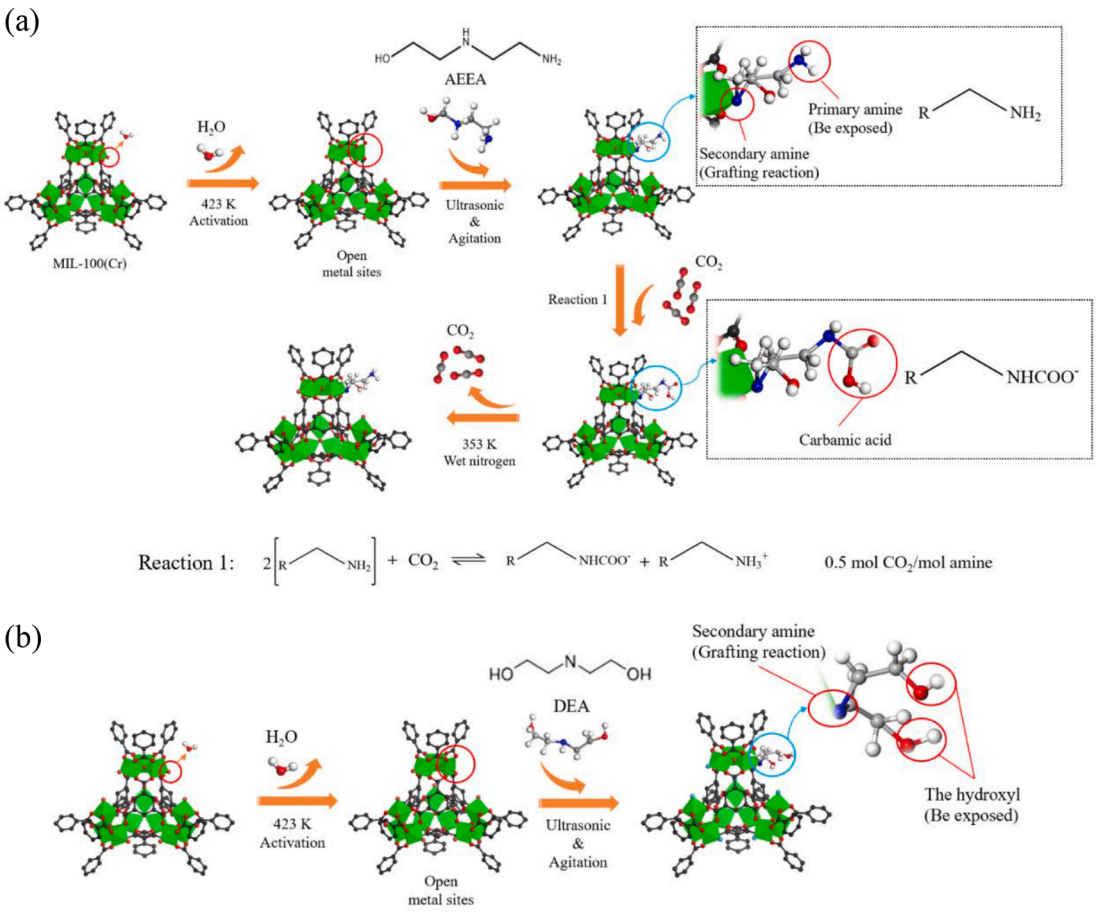

Fig. 1. Preparation, adsorption, and desorption schematic of MF-Cr-AEEA (a), DEA functional MIL-100(Cr) schematic (b) (black: carbon atoms for MIL-100(Cr), gray: carbon atoms for AEEA, red: oxygen atoms, green: chromium atoms, white: hydrogen atoms).

generate strong interactions between the metal and CO_2 [4]. Concurrently, most L and B acid sites can serve as sites for grafting amine groups preventing loss of amines resulting in their enhanced application in DAC technology [18–20]. The key to the grafting reaction is the physical and chemical properties of MOFs, including its specific surface area, pore size, surface functional groups, metal sites, pH, and CO_2 affinity. Meanwhile, the adsorption capacity, amine efficiency, temperature tolerance, and kinetics of adsorbents are restricted by MOFs properties. Thus, the amine grafting reaction principle and its constraints must be revisited to guide the study of MOFs amine adsorbents [19]. Moreover, for the study of CO_2 adsorption behavior on MOFs, the adsorption capacity, amine efficiency, and kinetics at ultra-low CO_2 partial pressure (400 ppm) are generally low and lack the experimental data of sub-ambient conditions (−30 to 20 °C), which severely hinders the large-scale implementation of MOFs adsorbent at DAC. So, to limit ultra-low partial pressures of CO_2, it is essential to improve adsorption performance and kinetics of the adsorbent at 400 ppm. Rim et al. [16] loaded poly(ethylenimine) (PEI) with MIL-101(Cr) to obtain an adsorbent with a high adsorption capacity of 1.81 mmol/g in the air at 25 °C. However, the amine efficiency of the adsorbent is only 0.14. Furthermore, the semi-adsorption time is more than 75 min, and the pseudo equilibrium time is 720 min, demonstrated extremely poor kinetic performance. Consequently, it is fascinating to develop new amine-functionalized MOFs with excellent CO_2 adsorption and kinetics performance at 400 ppm while revealing the grafting and adsorption mechanisms.

Based on these challenges, N-(2-aminoethyl)ethanolamine (AEEA) with low volatility is applied to functionalize MIL-100(Fe), UiO-66(Zr), and MIL-100(Cr) to synthesize the effective and reusable adsorbent. Preparation factors of types of MOFs and amines, the mass ratio of MIL-100(Cr) to AEEA(*M*), and the impregnating time (*t*) are investigated to obtain the optimal conditions. Meanwhile, to reveal the grafting mode of AEEA and explore the adsorption mechanism, the adsorbent is characterized using thermogravimetry analysis (TG), X-ray powder diffraction (XRD), Fourier transform infrared spectrometer (FTIR), scanning electron microscope (SEM), Energy Dispersive Spectrometer (EDS) and nitrogen adsorption–desorption. Additionally, the effect of adsorption temperature and water vapor concentration on adsorption performance is further investigated at an adsorption pressure of 400 ppm to obtain optimal adsorption parameters. While, the kinetic properties of the adsorbent, such as adsorption equilibrium constant and kinetic equation, have been derived from isotherms. Finally, the optimal desorption parameters and reusability are investigated to analyze energy consumption.

2. Experimental

2.1. Materials

Chromium(VI) oxide (CrO_3), hydrochloric acid (HCl), ethanol, and methanol were purchased from Sinopharm Chemical Reagent Co., Ltd. (Shanghai, China). N-(2-Aminoethyl) ethanolamine (AEEA) was obtained from Macklin Biochemical Co., Ltd. (Shanghai, China). Trimesic acid (H_3BTC) and deionized water were purchased from Aladdin Bio-Chem Technology Co., Ltd.

2.2. Preparation of MOFs

MIL-100(Cr) was prepared after modifications based on the available literature [16,21]. In detail, 2.13 g CrO_3 was mixed with 4.41 g H_3BTC at 100 mL deionized water. The mixture was then stirred magnetically at 60 °C for 1 h and transferred to a Teflon-lined steel autoclave reactor kept at 180 °C for four days. After that, the reactor was cooled to room temperature, and the mixture was centrifuged for precipitation. The precipitated solid was washed twice with 50 mL deionized water and 50 mL ethanol for 1 h at 50 °C and centrifuged, where the MIL-100(Cr) was obtained after being dried under vacuum at 120 °C for 5 h. Meanwhile, MIL-100(Fe) and UiO-66(Zr) were prepared directly based on the reported literature [17,22].

2.3. Adsorbent synthesis

A 0.5 g MOFs (MIL-100(Cr), MIL-100(Fe), or UiO-66(Zr)) was added to 10 mL absolute methanol and ultrasonically treated for 10 min. Then, based on the mass ratio of MOFs to AEEA (*M*), a certain mass of AEEA was added and ultrasound sealed for 20 min. Next, the mixture was stirred magnetically at room temperature for 12 h, defined as *t*. Finally, the mixture was purged with nitrogen at 70 °C for 1 h to dry solvent (MF-Cr/Fe/Zr-AEEA). The specific principle is outlined in Fig. 1.

2.4. Adsorbent characterizations

The crystal phase of the sample was recorded on Gemini A OHra X-ray powder diffraction (Oxford Diffraction, Co., Ltd., England), in which the monochromatic Cu k alpha radiation source was a tension of 40 kV and a current of 30 mA. The thermal stability of the sample was conducted on a TA-Q500 thermogravimetric analyzer (TA Instruments, Co., Ltd., America), conducted from 30 to 800 °C at a linear heating rate of 10 °C/min with 50 mL/min nitrogen flow. Functional groups of samples were measured by Nicolet iS50 FTIR spectroscopy (Thermo Fisher, Co., Ltd., America) with a spectral resolution of 4 cm^{-1} from 4000 to 400 cm^{-1}. The specific surface area, pore-volume, and pore diameter distribution of the adsorbent were determined with AUTOSORB-IQ2-MP (Quantachrome, Co., Ltd, America), and the sample was degassed for 8 h at 120 °C in a vacuum oven before the test. The surface morphology of the adsorbent was characterized using SU-8010 scanning electron microscopy (Hitachi Limited, Co., Ltd., Japan) operated at 2 kV. The element content and distribution of the adsorbent were analyzed on Energy Dispersive Spectrometer of X-max80 (Oxford Diffraction, Co., Ltd., England) and Elemental Analyzer of UNICUBE (Elementar, Co., Ltd., Germany). The pH of system was evaluated by pH meter. In detail, 0.2 g sample was mixed with 10 mL methanol and ultrasound treatment lasted for 10 min.

2.5. CO_2 adsorption experiment

The CO_2 adsorption experiment was conducted in an isothermal adsorption reactor, as shown in Fig. S1. The testing process included nitrogen purging and CO_2 adsorption. The adsorption capacity of CO_2 at a particular equilibrium concentration is calculated as Formula (1).

$$q_e = \frac{\sum V_{\text{in}} - c_e V_0}{m V_m} \tag{1}$$

Among them, q_e is equilibrium CO_2 capacity (mmol/g), c_e is the CO_2 concentration at equilibrium (ppm), $\sum V_{\text{in}}$ is the cumulative CO_2 injection amount (mL), V_0 is the reactor volume (mL), m is dry sample quality (g), V_m is the molar volume of gas (L/mol).

Amine efficiency is defined as the molar ratio of CO_2 adsorption capacity to amines (in terms of N), and the calculation equation is mentioned in Formula (2).

Table 1
Adsorption capacity of adsorbents with different types of MOFs and adsorbents.

MOFs and adsorbents	pH	Amines	Adsorption capacity (mmol/g)
MIL-100(Fe)	1.28	/	0.02
MF-Fe-AEEA	8.38	AEEA	0.29
UiO-66(Zr)	2.99	/	0.04
MF-Zr-AEEA	7.92	AEEA	0.08
MIL-100(Cr)	4.01	/	0.04
MF-Cr-AEEA	9.36	AEEA	2.05
MF-Cr-DEA	8.42	DEA	0.45

$$\eta_{\text{amine}} = \frac{q}{m_N} \tag{2}$$

Among them, q is the CO_2 adsorption capacity, mmol/g, m_N is the amount of amine (in terms of N) in adsorbent, mmol/g.

2.6. CO_2 desorption experiment

As revealed in Fig. 1a, the adsorbent after the adsorption experiment at 25 °C was purged with wet nitrogen of 3 L/min until CO_2 concentration fell below 5 ppm. Then, the temperature was increased to desorption temperature. The desorption process began until the concentration of CO_2 was again 5 ppm, indicating that the CO_2 was completely desorbed, and subsequent changes in carbon dioxide concentrations were recorded. After that, the adsorbent desorption was complete, which could then be placed in the isothermal adsorption test system for the next round.

2.7. Adsorption kinetics

The adsorption kinetics of the adsorbent was calculated by the pseudo-first-order kinetic equation and the pseudo-second-order kinetic equation to reveal the adsorption process [23,24]. The pseudo-first-order kinetic equation is mentioned in Formula (3), and the pseudo-second-order kinetic equation is mentioned in Formula (4).

$$q_t = q_e \cdot (1 - e^{-k_1 \cdot t}) \tag{3}$$

$$q_t = \frac{k_2 \cdot q_e^2 \cdot t}{1 + k_2 \cdot q_e \cdot t} \tag{4}$$

Among them, q_t is the adsorption capacity at time *t*, mmol/g, q_e is the adsorption capacity at equilibrium, mmol/g, k_1 and k_2 are the rate constant, min^{-1}.

3. Results and discussion

3.1. Amine grafting

To reveal the grafting/adsorption mechanism while optimizing the preparation factors, effects of MOFs and amines, the mass ratio of MIL-100(Cr) to AEEA (*M*), and impregnating time (*t*) on the adsorptive property were investigated, while the adsorptive parameter was set as adsorption temperature of 25 °C, CO_2 concentration of 400 ppm and water vapor concentration of 1 %.

3.1.1. Effects of MOFs and amines

Depending on the choice of metal ions, MOFs can obtain various surface characteristics and rich L acid sites, which can be described in terms of the magnitude of pH [4,17]. Thus, to reveal the amine grafting reaction principle and its constraints, MIL-100(Fe), UiO-66(Zr), and MIL-100(Cr) with different metal acid sites and pH were investigated at $M = 1{:}1$, $t = 12$ h. As indicated in Table 1, the adsorption capacity of MIL-100(Fe), UiO-66(Zr), and MIL-100(Cr) was recorded as 0.02, 0.04, and 0.04 mmol/g, respectively, demonstrating poor adsorption

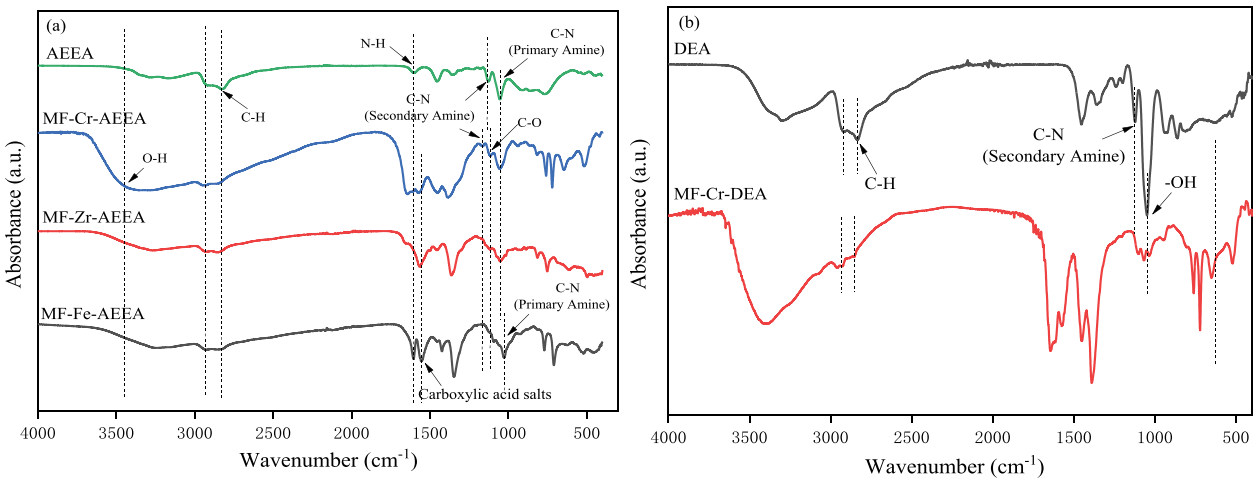

Fig. 2. FTIR spectra of amines and its MOFs adsorbents.

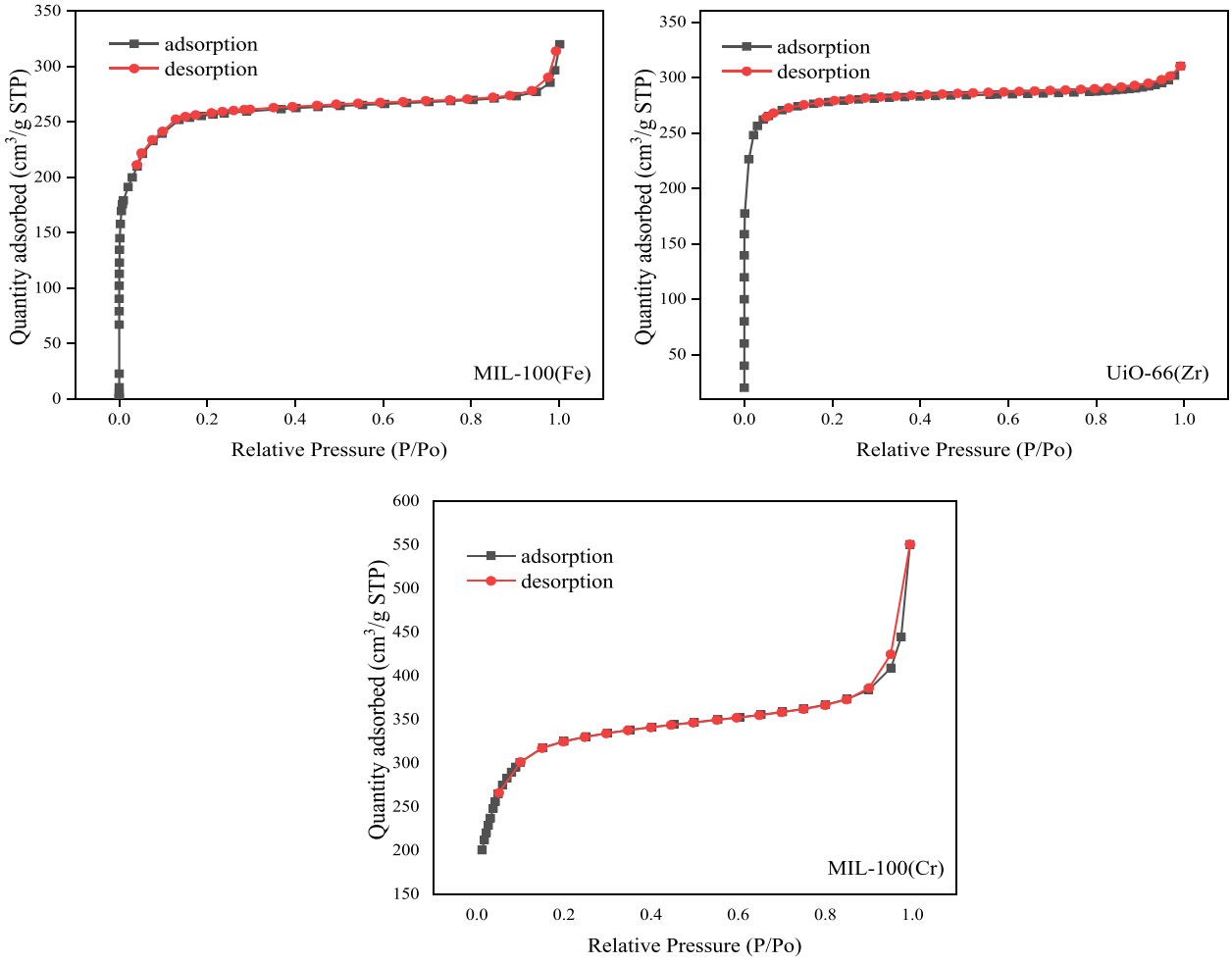

Fig. 3. Nitrogen adsorption–desorption isotherm of MIL-100(Fe), UiO-66(Zr), and MIL-100(Cr).

performance of MOFs from atmospheric pressure. After functionalization with AEEA, the adsorption capacity of MF-Fe-AEEA, MF-Cr-AEEA, and MF-Zr-AEEA were increased to 0.29, 2.05, 0.08 mmol/g, respectively. Among them, the adsorption capacity of MF-Cr-AEEA was the largest, demonstrating the efficient linking between Cr metal sites and amine groups [25,26]. The pH of MIL-100(Cr) was 4.01, the highest among MOFs, indicating that low pH was not conducive to the collaborative adsorption of metal sites and amine groups due to the neutralization reaction.

From Fig. 2(a), the C—N stretching vibration bands of the primary and secondary amine groups were detected at around 1170 and 1057 cm^{-1} in MF-Cr-AEEA, MF-Zr-AEEA, and MF-Fe-AEEA because AEEA owns both primary and secondary amine groups [27,28]. However, it is worth noting that the C—N band intensity of the secondary amine group

Table 2
Specific surface area, average pore size, and pore volume of MIL-100(Fe), UiO-66(Zr), and MIL-100(Cr).

MOFs	Specific surface area (m^2/g)	Average pore size (nm)	Pore volume (m^3/g)
MIL-100 (Fe)	1103	1.68	0.62
UiO-66 (Zr)	861	2.16	0.46
MIL-100 (Cr)	1269	1.34	0.85

decreased significantly in MF-Cr-AEEA, while it almost disappeared in MF-Zr-AEEA and MF-Fe-AEEA. Meanwhile, the primary amine group remained unchanged. It has been demonstrated that the grafting process is the reaction between metal acid sites and secondary amines, while the exposed primary amines function as the active site for CO_2 adsorption (Fig. 1) [29]. This could be attributed to the higher adsorption energy of secondary amines with higher alkalinity than primary amines for metal sites [25,26].

Moreover, the bands at 2825 and 2930 cm^{-1} were C—H vibration bands, while the absorption band of O—H was widened due to the absorption of moisture from the air. The characteristic asymmetric stretching absorption peak of carboxylic acid salts at 1560 cm^{-1} and C—O at 1120 cm^{-1} were recorded due to the existence of MOFs. However, the absorption peak intensity of N—H around 1600 cm^{-1} declined in MF-Fe-AEEA, and it disappeared in MF-Zr-AEEA, resulting in poor adsorption performance. Due to the considerable acidity of Fe and Zr metallic acid sites, primary amines and secondary amines of AEEA all participate in the grafting reaction, resulting in the loss of active adsorption sites (Table 1). To sum up, amine-modified MOFs is a coupling process of chemical grafting with physical filling, making full use of the high specific surface area and pore volume characteristics of MOFs which provides a chemical grafting reaction interface and a physical filling site.

In addition, as displayed in Fig. 3, the illustrated isotherms for MOFs are assigned to a type I pattern characteristic of microporous structures [17]. As depicted in Table 2, the higher surface area (1269 m^2/g) and pore volume (0.85 m^3/g) of MIL-100(Cr) than UiO-66(Zr) and MIL-100 (Fe) [25]. Based on the high porosity of MIL-100(Cr), the CO_2 binding energy of surface functional groups and pH can be adjusted by chemical modification to obtain good adsorption and desorption properties. Therefore, MIL-100(Cr) functionalized by the AEEA became the subject of further research. Moreover, from Fig. S2 and Fig. S3, the optimized preparation factors are the mass ratio of MIL-100(Cr) to AEEA as 1:1 and impregnating time as 12 h.

To modify MIL-100(Cr), diethanolamine (DEA), mostly composed of secondary amines, has an adsorption capacity of 0.49 mmol/g. To uncover the reason, the FTIR spectra of DEA and MF-Cr-DEA are demonstrated in Fig. 2(b). The band of C—N at 1140 cm^{-1} and –OH deformation vibrations at 1050 cm^{-1} have been recorded in DEA. After the grafting procedure, the band of C—N disappeared, and –OH is decreased in MF-Cr-DEA. This could be attributed to the reaction between the secondary amine group in DEA and Cr metal vacancy (Fig. 1 (b)). Hence, amines possessing a variety of amine groups in their structure were preferred because of their high adsorption performance.

3.2. Adsorption performance

3.2.1. Effect of adsorption temperature

The optimal adsorbent temperature of MF-Cr-AEEA was further investigated at a CO_2 concentration of 400 ppm and a water vapor concentration of 1 %. As seen in Fig. 4(a), the adsorption capacity of 1.91 mmol/g and efficiency of the amine of 0.20 was achieved at −25 °C. As the temperature was raised to 0 °C, the adsorption capacity and amine efficiency reached the maximum of 2.42 mmol/g and 0.25, respectively. However, it monotonously decreased if the adsorption temperature was further increased, and the adsorption capacity of 0.60 mmol/g and efficiency of the amine of 0.06 was obtained at 50 °C. According to the literature [16,30], the heat and mass transfer rate of CO_2 and adsorbent was decreased due to the low adsorption temperature, leading to an increase in semi-adsorption time (Fig. S4(a)) and the reduction of adsorption capacity. Meanwhile, some of the water vapor can condense at −25 °C, blocking the adsorbent pores and reducing the physical diffusion surfaces. And, the molecular mobility was decreased that results in dramatically lower accessibility of the gas phase CO_2 to the amine groups or to there being insufficient thermal energy available to surpass chemisorption activation barriers [16]. However, excessive adsorption temperatures affect the adsorption of CO_2 under partial pressure, reducing the adsorbent's affinity for CO_2 [19,31,32]. In addition, due to the reaction of CO_2 with amino groups is exothermic, the equilibrium of the adsorption reaction shifts in the direction of desorption as the temperature increases. The best attribute of an adsorbent is its excellent adsorption performance at sub-ambient conditions, which allows it to be deployed in extreme weather conditions.

TG curves of MIL-100(Cr) and MF-Cr-AEEA are obtained from Fig. S5 to analyze thermal stability under high adsorption temperatures. The TG curve of MIL-100(Cr) and MF-Cr-AEEA exhibits three stages of mass loss. The first stage is the surface moisture loss when the temperature is less than 100 °C [33,34]. The mass loss (13 %) of MIL-100(Cr) between 100 and 400 °C is the second stage which could be due to the removal of bound water and extra ligand in the crystal structure [33–35]. In

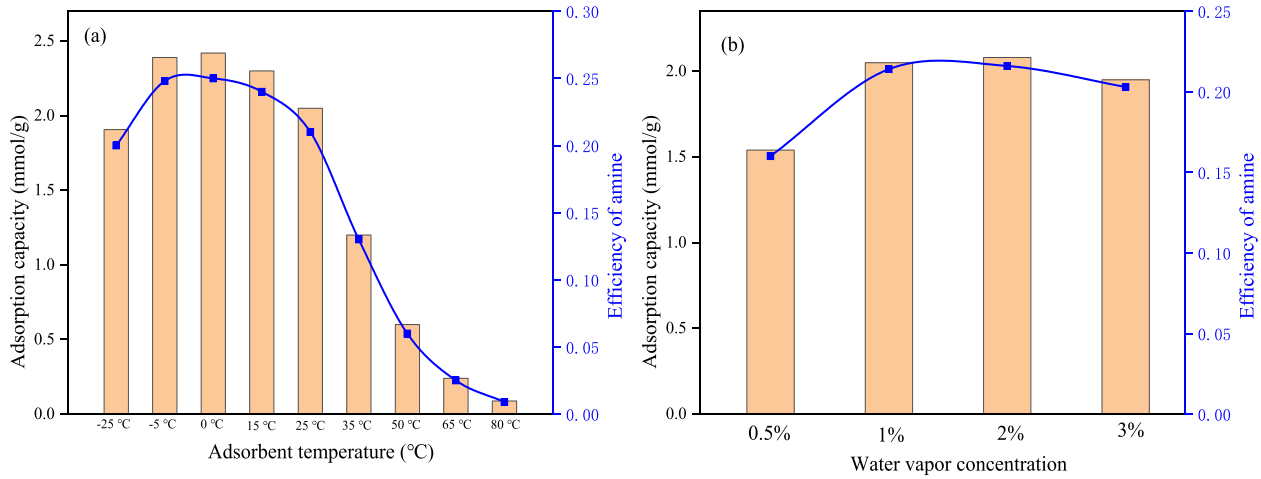

Fig. 4. Adsorption capacity of adsorbents with different adsorption temperatures and water vapor concentrations.

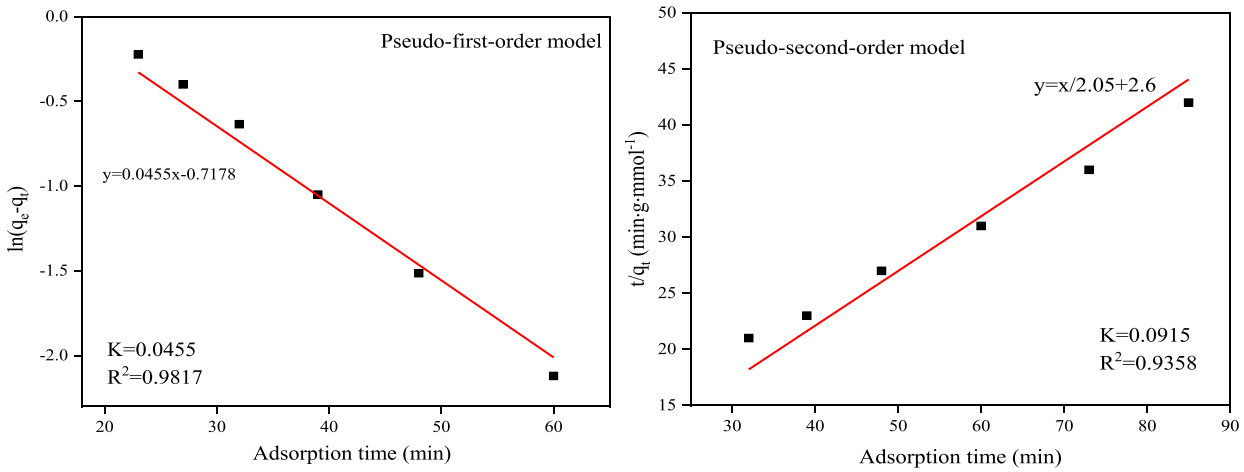

Fig. 5. Pseudo-first-order and pseudo-second-order kinetic equation fitting curves of MF-Cr-AEEA at 25 °C.

contrast to MIL-100(Cr) decomposition, the second mass loss of MF-Cr-AEEA is about 40 % from 100 to 350 °C due to the decomposition of carbonate and carbamate. A significant mass loss was detected from MIL-100(Cr) and MF-Cr-AEEA between 400 and 600 °C because MOFs structure was damaged, demonstrating the high thermal stability of the adsorbent. The weightlessness remains almost constant when the temperature exceeds 600 °C. Moreover, MIL-100(Cr) calcination residue exceeds that of MF-Cr-AEEA, corroborating the insertion of AEEA, consistent with FTIR.

3.2.2. *Effect of water vapor concentration*

The effect of water vapor concentration was further investigated at an adsorption temperature of 25 °C. As seen in Fig. 4(b) and Fig. S4(b), the adsorption capacity of 1.54 mmol/g and efficiency of the amine of 0.16 was achieved when the water vapor concentration is 0.5 %. Further increased water vapor concentration to 1 %, the adsorption capacity was improved to 2.05 mmol/g, and the semi-adsorption time declined to 18 min, which is because the presence of water provides abundant active sites for the adsorption reaction [36]. As the water vapor concentration increased to 3 %, the adsorption capacity declined slightly to 1.95 mmol/g, and the semi-adsorption time increased to 19 min. It could be because condensation of water causes blockage of the adsorbent channel, affecting the exposure of the active site. Due to the adsorption capacity being stable when the concentration of water vapor exceeds 1 %, a water vapor concentration of 1 % was used in the follow-up study.

3.2.3. *Adsorption kinetics*

To further reveal the adsorption process, pseudo-first-order and pseudo-second-order kinetic equation fitting curves of MF-Cr-AEEA at adsorption temperature of 25 °C and water vapor concentration of 1 % are recorded (Fig. 5). Theoretically, the pseudo-second-order kinetic model assumes that the adsorption rate is determined by the square value of the number of adsorbed vacancies on the surface of the adsorbent that is not occupied, and it involves electron sharing or electron transfer between the adsorbent and CO_2 [37]. That is to say, the pseudo-second-order kinetic model is controlled by the mechanism of chemical adsorption. Due to the high fitting effect of pseudo-first-order and pseudo-second-order kinetic equations, it is proved that the adsorption rate of CO_2 is controlled by both surface diffusion and chemical reactions [37]. Yet it is worth noting that, due to the thermodynamics of the reaction, the equilibrium of the adsorption reaction shifts in the direction of desorption as the temperature increases, so adsorption amounts decrease rapidly. This phenomenon proves that the adsorption process is mainly determined by chemical adsorption.

In addition, in general, the reaction of CO_2 with amino groups is exothermic, but the reaction at different temperatures is a competitive process between thermodynamics and kinetics. To further reveal the effect of temperature, pseudo-first-order kinetic equation fitting curves with different adsorption temperatures are analyzed (Fig. S6). From Table S1 and Fig. S4, with the increase of the adsorption temperature, the adsorption rate of the adsorbent showed an upward trend, and the semi-adsorption times are all below 21 min, demonstrating the rapid heat and mass transfer process in MF-Cr-AEEA. It is because the activity of CO_2 molecules enhances with the increase of temperature, which is conducive to the diffusion of CO_2 inside the adsorbent pores [37].

The exceptional structure of the adsorbent is the key to improving adsorption kinetics. The crystal structure changes of MIL-100(Cr) and MF-Cr-AEEA were investigated by X-ray powder diffraction. From Fig. S7, the diffraction peaks at $2\theta = 6.3°$, 10.9°, 14.5°, 18.8°, 20.2°, and 24.3° are the standard peaks of MIL-100(Cr), proving that the synthesized sample is the highly crystalline MIL-100(Cr) [38]. After grafting AEEA, the diffraction pattern of MF-Cr-AEEA is consistent with that of MIL-100(Cr), indicating that the maintained crystal structure after loading results in splendid kinetics performance, as shown in Table S1. The intensity of the diffraction peaks at $2\theta = 6.3°$ and 14.5° was decreased, possibly due to the insertion of AEEA changed electron density [38]. In addition, the surface morphology of MF-Cr-AEEA was characterized as shown in Fig. S8(a). The results showed that the surface morphology of MF-Cr-AEEA resembled a flake structure with a uniform distribution. Meanwhile, as numbers of small particles were agglomerated into a cluster, the overall size found of MF-Cr-AEEA was 30 μm.

To further reveal the principle of improving kinetics performance, the nitrogen adsorption–desorption isotherm of MF-Cr-AEEA was obtained, as shown in Fig. S9. Based on the IUPAC classification, the isotherm has been ascribed to type IV, indicating that MF-Cr-AEEA was subjected to mesoporous materials [33,39]. To confirm the result, the Brunauer-Emmett-Teller (BET) specific surface area, average pore size, and pore volume were also analyzed, where they were concentrated on 6.67 m^2/g, 25.82 nm, and 0.086 m^3/g, respectively (Table S2). Compared with MIL-100(Cr) in Table 2, although the specific surface area and pore volume of MF-Cr-AEEA decreased, the outstanding kinetics performance and the high amine efficiency were obtained via adsorption experiments compared with the same type of adsorbents. Moreover, the average pore size increased, which may be attributed to the grafted AEEA molecules changing MOFs channel structure, facilitating the gas–solid mass transfer in the adsorbent. This is also an important demonstration of the reaction between chromium vacancy sites and secondary amines, which is the same as FTIR.

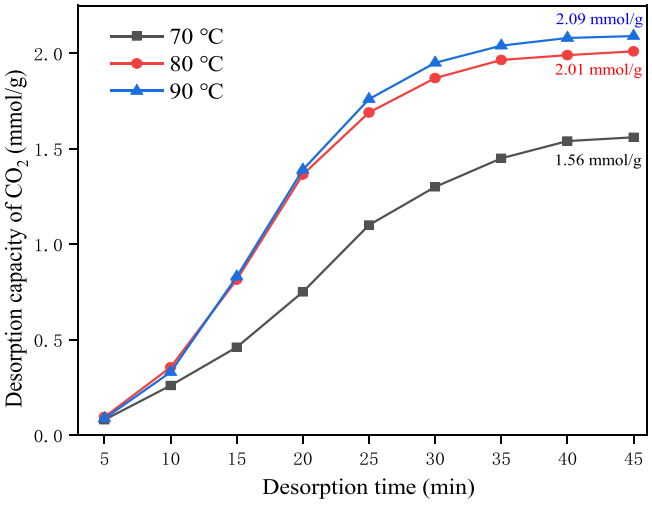

Fig. 6. Effect of time and temperature on MF-Cr-AEEA desorption.

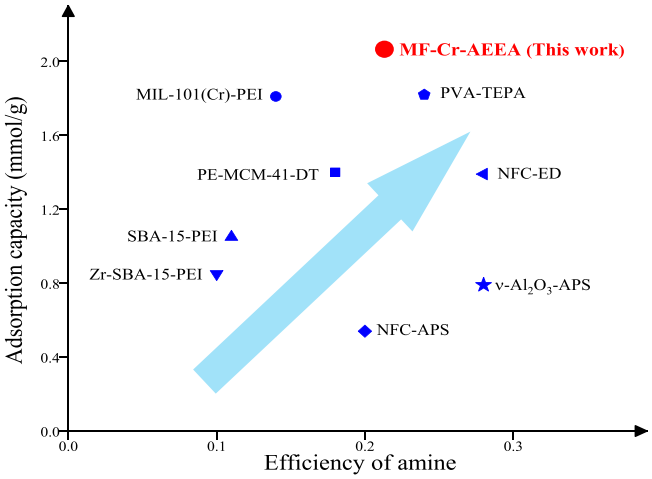

Fig. 7. CO_2 adsorption capacity and efficiency of amine of MF-Cr-AEEA and other DAC adsorbents [16,40,41].

3.3. Desorption performance

3.3.1. Effect of time and temperature

To demonstrate the influence of time and temperature on desorption, the CO_2 desorption capacity of the adsorbent after adsorption at 25 °C was recorded, as shown in Fig. 6. When the desorption temperature reached 70 °C, the low desorption capacity of 0.08 mmol/g was detected due to the low heat and mass transfer in the adsorbent at 5 min. When the desorption time increased, the adsorbent's internal temperature increased, so the desorption capacity was significantly improved, especially within a short span of 30 min. After 45 min, the desorption capacity was 1.56 mmol/g, which confirmed incomplete desorption. As the temperature was increased to 80 °C, the maximum desorption increased to 2.01 mmol/g, and the complete desorption time decreased. This is because elevated temperature improves heat and mass transfer inside the adsorbent.

Further increase in desorption temperature to 90 °C led to a slight increase to 2.09 mmol/g in the amount of CO_2 desorption, which is slightly higher than the adsorption experiment (2.05 mmol/g). Firstly, the desorption data are obtained by integrating the experimental data, which may lead to the existence of experimental errors. Secondly, when the adsorbent is placed on adsorption bed and the adsorption system begins to purge, the adsorbent may come into contact with some CO_2 in the air, which cannot be recorded by the adsorption system, resulting in a slightly higher amount of desorption in the high-temperature desorption experiment than in the adsorption experiment.

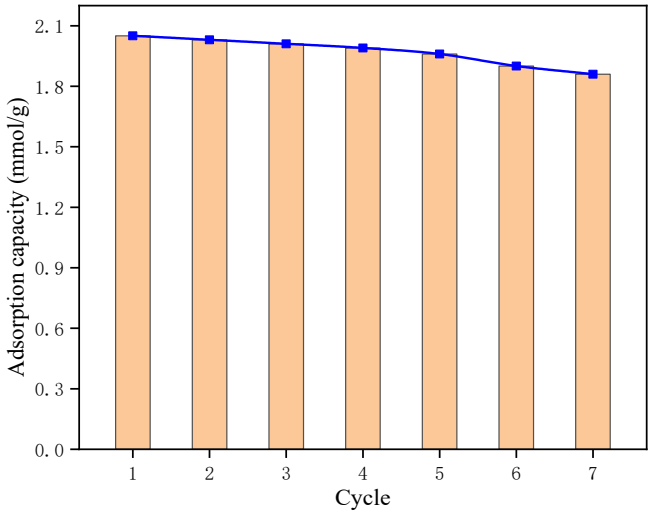

Fig. 8. Reusability of MF-Cr-AEEA (adsorption temperature of 25 °C).

From Table 1, the pH of MF-Cr-AEEA is 9.36, which is lower than the pH of AEEA (pH = 11.16). It proves that the CO_2 binding energy after the grafting reaction is weakened, which is beneficial to reduce the desorption temperature. In addition, from Fig S10, the semi-desorption time are all below 20 min and the complete desorption time are all about 40 min, which is attributed to the high kinetic performance. Thus, to save energy and ensure complete desorption, the optimal desorption temperature and time were set as 80 °C and 40 min, respectively.

Generally, the adsorption or desorption performance and energy consumption are challenges for adsorbents, affecting the economic efficiency of CO_2 adsorption. As shown in Fig. 7, the CO_2 adsorption capacity and efficiency of the amine of MF-Cr-AEEA at 25 °C were 2.05 mmol/g and 0.21, respectively, and the desorption temperature was only 80 °C, demonstrating better performance and less-energy of MF-Cr-AEEA compared with other DAC adsorbents reported in the literature [16,40,41].

3.4. Adsorbent reusability

This study conducted MF-Cr-AEEA reusability analysis by purging wet nitrogen at 80 °C. As presented in Fig. 8, an adsorption capacity of 2.05 mmol/g was obtained in the first cycle and slowly declined with the repetition cycle. The adsorption capacity remained at 1.86 mmol/g and the semi-adsorption time remained at 20.3 min up to the seventh cycle (Fig. S11). To identify the underlying reason, the MF-Cr-AEEA-Seventh cycle was characterized by X-ray powder diffraction (XRD), Fourier transform infrared spectrometer (FTIR), scanning electron microscope (SEM), Energy Dispersive Spectrometer (EDS), and nitrogen adsorption–desorption. Combined with XRD and SEM of MF-Cr-AEEA-Seventh cycle shown in Figs. S7 and S8b, the characteristic crystal diffraction peak and surface morphology of MF-Cr-AEEA were still maintained proved the structural stability of the adsorbent.

Additionally, from Fig. S12, it has been found that the strong characteristic absorption peaks of AEEA were recorded in the infrared spectra of the MF-Cr-AEEA-Seventh cycle. Meanwhile, the characteristic absorption peak of carbamate was detected around 1650 cm^{-1}, and the peaks of carbonate were recorded around 850 cm^{-1} and 700 cm^{-1}. This indicated that a small amount of carbamate and carbonate still failed to decompose under regeneration conditions of 40 min at 80 °C. If the desorption time is prolonged, the carbamate and carbonate could be completely decomposed. In addition, it should be noted that BET surface

Table 3
Elemental Analysis of MF-Cr-AEEA and MF-Cr-AEEA-Seventh cycle.

Adsorbent	C (%)	H (%)	O (%)	N (%)	Cr (%)
MF-Cr-AEEA	38.1	5.63	34.29	11.79	10.19
MF-Cr-AEEA-Seventh cycle	39.31	4.87	34.15	10.88	10.79

area was decreased to 3.2 m^2/g after seven cycles (Fig. S9). This could be because the carbonates and carbamate formed during the adsorption process occupied the space inside the pores (Fig. S12), which is one of the reasons for the decrease in adsorption capacity.

Moreover, the high elemental dispersion was maintained from the EDS spectrum of Fig. S13, indicating the high chemical stability. However, from Elemental Analysis (EA) in Table 3, the elemental ratio of N was decreased, demonstrating the loss of AEEA during regeneration, resulting in a slight decrease in cyclic adsorption capacity. And, due to the loss of some AEEA, the total number of atoms in the adsorbent molecules decreased, so that, the elemental ratio of Cr was increased slightly.

4. Conclusions

In this study, MIL-100(Fe), UiO-66(Zr), and MIL-100(Cr) were functionalized using N-(2-Aminoethyl)ethanolamine through the post-functionalization method. The results showed that the grafting process is the reaction between metallic vacancy sites and secondary amines of AEEA; the exposed primary amine acts as the active site for CO_2 adsorption. Compared with the Fe and Zr, abundant coordinatively unsaturated Cr cations in MIL-100(Cr) effectively promote amine grafting without destroying the active site because of the high surface area, pore volume, and pH. Moreover, the optimal preparation factors of MF-Cr-AEEA were obtained as $M = 1$, $t = 12$ h, which exhibited high CO_2 capacity (2.05 mmol/g) at 400 ppm of CO_2 among most MOFs. According to the characterizations, the grafting process is the reaction between metal vacancy sites and secondary amines, resulting in excellent structural stability. Thus, amine owning more types of amine groups in the structure are preferred for grafting. Meanwhile, the results of EDS showed the uniform distribution of amine groups within the adsorbent, indicating the homogeneity of the adsorbent. From adsorption experiments, the adsorbent has demonstrated excellent temperature tolerance and is found to be thermally stable up to 400 °C. Moreover, MF-Cr-AEEA maintained the MIL-100(Cr) crystal texture after functionalization, and the average pore size was 25.82 nm. Based on the outstanding structural characteristics, the excellent kinetics performance of MF-Cr-AEEA resulted from the low semi-adsorption times below 21 min. Meanwhile, the optimal desorption temperature and time were 80 °C and 40 min, respectively, indicating the low renewable energy consumption. The adsorption capacity after the seventh cycle remained at 1.86 mmol/g, which proved the splendid cycling stability of the adsorbent and the possibility of industrial application.

Declaration of Competing Interest

The authors declare that they have no known competing financial interests or personal relationships that could have appeared to influence the work reported in this paper.

Data availability

No data was used for the research described in the article.

Acknowledgements

This work is supported by Natural Science Foundation for Young Scientists of Zhejiang Province, No.LR19E060002; National Natural Science Foundation of China, No.51676169; Fundamental Research Funds for the Central Universities (2022ZFJH004, 2021XZZX012).

Appendix A. Supplementary data

Supplementary data to this article can be found online at https://doi.org/10.1016/j.cej.2022.140431.

References

[1] S. Kazemi, V. Safarifard, Carbon dioxide capture in MOFs: the effect of ligand functionalization, Polyhedron 154 (2018) 236–251, https://doi.org/10.1016/j.poly.2018.07.042.
[2] A. Zulys, F. Yulia, N. Muhadzib, Nasruddin, Biological metal-organic frameworks (bio-mofs) for co$_2$ capture, Ind. Eng. Chem. Res. 60 (1) (2021) 37–51, https://doi.org/10.1021/acs.iecr.0c04522.
[3] E.S. Sanz-Perez, C.R. Murdock, S.A. Didas, C.W. Jones, Direct capture of co$_2$ from ambient air, Chem. Rev. 116 (19) (2016) 11840–11876, https://doi.org/10.1021/acs.chemrev.6b00173.
[4] W.R. Lee, S.Y. Hwang, D.W. Ryu, K.S. Lim, S.S. Han, D. Moon, J. Choi, C.S. Hong, Diamine-functionalized metal-organic framework: exceptionally high CO_2 capacities from ambient air and flue gas, ultrafast CO_2 uptake rate, and adsorption mechanism, Energy Environ. Sci. 7 (2) (2014) 744–751, https://doi.org/10.1039/c3ee42328j.
[5] C. Kim, H.S. Cho, S. Chang, S.J. Cho, M. Choi, An ethylenediamine-grafted Y zeolite: a highly regenerable carbon dioxide adsorbent via temperature swing adsorption without urea formation, Energy Environ. Sci. 9 (5) (2016) 1803–1811, https://doi.org/10.1039/c6ee00601a.
[6] S.K. Wahono, A.A. Dwiatmoko, A. Cavallaro, S.C. Indirathankam, J. Addai-Mensah, W. Skinner, A. Vinu, K. Vasilev, Amine-functionalized natural zeolites prepared through plasma polymerization for enhanced carbon dioxide adsorption, PLASMA PROCESSES POLYM. 18 (8) (2021), https://doi.org/10.1002/ppap.202100028.
[7] Z.X. Li, Q.H. Wang, Y. Feng, M.X. Fang, Experiments and DFT study on modified CaO-based adsorbents for enhanced CO_2 capture, C. R. Chim. 24 (2) (2021) 177–187, https://doi.org/10.5802/crchim.79.
[8] Y. Bang, S.J. Han, S. Kwon, V. Hiremath, I.K. Song, J.G. Seo, High temperature carbon dioxide capture on nano-structured MgO-Al_2O_3 and CaO-Al_2O_3 adsorbents: an experimental and theoretical study, J. NANOSCI. NANOTECHNOL. 14 (11) (2014) 8531–8538, https://doi.org/10.1166/jnn.2014.9954.
[9] N. Alvarez-Gutierrez, M.V. Gil, F. Rubiera, C. Pevida, Cherry-stones-based activated carbons as potential adsorbents for CO_2/CH_4 separation: effect of the activation parameters, GREENHOUSE GASES-SCI. TECHNOL. 5 (6) (2015) 812–825, https://doi.org/10.1002/ghg.1534.
[10] H.R. Penchah, A. Ghaemi, F. Jafari, Piperazine-modified activated carbon as a novel adsorbent for CO_2 capture: modeling and characterization, ENVIRONMENTAL SCIENCE AND POLLUTION RESEARCH. https://doi.org/10.1007/s11356-021-16040-5.
[11] W.J. Wang, F.L. Liu, Q.X. Zhang, G. Yu, S.B. Deng, Efficient removal of CO_2 from indoor air using a polyethyleneimine-impregnated resin and its low-temperature regeneration, Chem. Eng. J. 399 (2020), https://doi.org/10.1016/j.cej.2020.125734.
[12] Z.H. Chen, S.B. Deng, H.R. Wei, B. Wang, J. Huang, G. Yu, Polyethylenimine-impregnated resin for high co$_2$ adsorption: an efficient adsorbent for co$_2$ capture from simulated flue gas and ambient Air, ACS Appl. Mater. Interfaces 5 (15) (2013) 6937–6945, https://doi.org/10.1021/am400661b.
[13] M. Badanicova, V. Zelenak, Organo-modified mesoporous silica for sorption of carbon dioxide, Monatsh. Chem. 141 (6) (2010) 677–684, https://doi.org/10.1007/s00706-010-0304-6.
[14] M. Mohamedali, H. Ibrahim, A. Henni, Imidazolium based ionic liquids confined into mesoporous silica MCM-41 and SBA-15 for carbon dioxide capture, Microporous Mesoporous Mater. 294 (2020), 109916, https://doi.org/10.1016/j.micromeso.2019.109916.
[15] J.M. Findley, D.S. Sholl, Computational screening of mofs and zeolites for direct air capture of carbon dioxide under humid conditions, J. Phys. Chem. C 125 (44) (2021) 24630–24639, https://doi.org/10.1021/acs.jpcc.1c06924.
[16] G. Rim, F. Kong, M. Song, C. Rosu, P. Priyadarshini, R.P. Lively, C.W. Jones, Sub-ambient temperature direct air capture of co$_2$ using amine-impregnated mil-101 (cr) enables ambient temperature co$_2$ recovery, JACS Au 2 (2) (2022) 380–393, https://doi.org/10.1021/jacsau.1c00414.
[17] F.S. Liu, X.L. Ma, H. Li, Y.Y. Wang, P. Cui, M. Guo, H.L. Yaxin, W.P. Lu, S.J. Zhou, M.Z. Yu, Dilute sulfonic acid post functionalized metal organic framework as a heterogeneous acid catalyst for esterification to produce biodiesel, Fuel 266 (2020), https://doi.org/10.1016/j.fuel.2020.117149.
[18] H. Li, F.S. Liu, X.L. Ma, P. Cui, M. Guo, Y. Li, Y. Gao, S.J. Zhou, M.Z. Yu, An efficient basic heterogeneous catalyst synthesis of magnetic mesoporous Fe@C support SrO for transesterification, Renewable Energy 149 (2020) 816–827, https://doi.org/10.1016/j.renene.2019.12.118.
[19] T.M. McDonald, W.R. Lee, J.A. Mason, B.M. Wiers, C.S. Hong, J.R. Long, Capture of carbon dioxide from air and flue gas in the alkylamine-appended metal-organic framework mmen-mg-2(dobpdc), J. Am. Chem. Soc. 134 (16) (2012) 7056–7065, https://doi.org/10.1021/ja300034j.
[20] Z. Li, P. Liu, C. Ou, X. Dong, Porous metal-organic frameworks for carbon dioxide adsorption and separation at low pressure, ACS Sustainable Chem. & Eng. 8 (41) (2020) 15378–15404, https://doi.org/10.1021/acssuschemeng.0c05155.

[21] P. Miao, G. Li, G. Zhang, H. Lu, Co(II)-salen complex encapsulated into MIL-100 (Cr) for electrocatalytic reduction of oxygen, J. Energy Chem. 23 (4) (2014) 507–512, https://doi.org/10.1016/S2095-4956(14)60178-9.
[22] F.G. Cirujano, A. Corma, F. Xamena, Conversion of levulinic acid into chemicals: synthesis of biomass derived levulinate esters over Zr-containing MOFs, Chem. Eng. Sci. 124 (2015) 52–60, https://doi.org/10.1016/j.ces.2014.09.047.
[23] Y. Pan, Y. Wang, W. Liu, B. Zhao, B. Chen, Adsorption kinetics and thermodynamics of adn on activated carbon, Chin. J. Explosives Propellants 42 (5) (2019) 465–472. https://doi.org/10.14077/j.issn.1007-7812.2019.05.008.
[24] Y.X. Han, Study on the Modification and Decarbonization Properties of 13X molecular sieve and silica gel [D], Univ.of Shandong Jianzhu, China, 2021 https://doi.org/10.27273/d.cnki.gsajc.2021.000269.
[25] S.K. Xian, J.J. Peng, Z.J. Zhang, Q.B. Xia, H.H. Wang, Z. Li, Highly enhanced and weakened adsorption properties of two MOFs by water vapor for separation of CO_2/CH_4 and CO_2/N_2 binary mixtures, Chem. Eng. J. 270 (2015) 385–392, https://doi.org/10.1016/j.cej.2015.02.041.
[26] L.-B. Zhao, R. Huang, M.-X. Bai, D.-Y. Wu, Z.-Q. Tian, Effect of aromatic amine−metal interaction on surface vibrational raman spectroscopy of adsorbed molecules investigated by density functional theory, J. Phys. Chem. C 115 (10) (2011) 4174–4183, https://doi.org/10.1021/jp1117135.
[27] K. Krishnan, R.A. Plane, Raman and infrared spectra of complexes of ethylenediamine with zinc(ii), cadmium(ii), and mercury(II), Inorg. Chem. 5 (5) (1966) 852–857, https://doi.org/10.1021/ic50039a031.
[28] D.A. Young, T.B. Freedman, E.D. Lipp, L.A. Nafie, VIBRATIONAL CIRCULAR-DICHROISM IN TRANSITION-METAL COMPLEXES .2. ION ASSOCIATION, RING CONFORMATION, AND RING CURRENTS OF ETHYLENEDIAMINE LIGANDS, JOURNAL OF THE AMERICAN CHEMICAL SOCIETY 108(23) (1986) 7255-7263. https://doi.org/10.1021/ja00283a021.
[29] C.P. Cabello, G. Berlier, G. Magnacca, P. Rumori, G.T. Palomino, Enhanced CO_2 adsorption capacity of amine-functionalized MIL-100(Cr) metal-organic frameworks, CrystEngComm 17 (2) (2015) 430–437, https://doi.org/10.1039/c4ce01265h.
[30] L. Wang, F.F. Zhang, C. Wang, Y. Li, J.F. Yang, L.B. Li, J.P. Li, Ethylenediamine-functionalized metal organic frameworks MIL-100(Cr) for efficient CO_2/N_2O separation, SEP. PURIF. TECHNOL. 235 (2020), https://doi.org/10.1016/j.seppur.2019.116219.
[31] N. Al-Janabi, H.R. Deng, J. Borges, X.F. Liu, A. Garforth, F.R. Siperstein, X.L. Fan, A facile post-synthetic modification method to improve hydrothermal stability and co_2 selectivity of cubtc metal-organic framework, Ind. Eng. Chem. Res. 55 (29) (2016) 7941–7949, https://doi.org/10.1021/acs.iecr.5b04217.
[32] P.M. Bhatt, Y. Belmabkhout, A. Cadiau, K. Adil, O. Shekhah, A. Shkurenko, L. J. Barbour, M. Eddaoudi, A Fine-tuned fluorinated mof addresses the needs for trace co_2 removal and air capture using physisorption, J. Am. Chem. Soc. 138 (29) (2016) 9301–9307, https://doi.org/10.1021/jacs.6b05345.
[33] S.I. Kim, T.U. Yoon, M.B. Kim, S.J. Lee, Y.K. Hwang, J.S. Chang, H.J. Kim, H.N. Lee, U.H. Lee, Y.S. Bae, Metal-organic frameworks with high working capacities and cyclic hydrothermal stabilities for fresh water production, Chem. Eng. J. 286 (2016) 467–475, https://doi.org/10.1016/j.cej.2015.10.098.
[34] S. Rostamnia, F. Mohsenzad, Nanoarchitecturing of open metal site Cr-MOFs for oxodiperoxo molybdenum complexes [$MoO(O_2)$(2)@En/MIL-100(Cr)] as promising and bifunctional catalyst for selective thioether oxidation, MOLECULAR CATALY. 445 (2018) 12–20, https://doi.org/10.1016/j.mcat.2017.11.003.
[35] J.M. Fernandez-Morales, L.A. Lozano, E. Castillejos-Lopez, I. Rodriguez-Ramo, A. Guerrero-Ruiz, J.M. Zamaro, Direct sulfation of a Zr-based metal-organic framework to attain strong acid catalysts, MICROPOROUS MESOPOROUS MATER. 290 (2019), https://doi.org/10.1016/j.micromeso.2019.109686.
[36] Z.L. Liu, Preparation and CO_2 Adsorption Performance of Amine-functionalized MCM-41[D], Univ.of North China Electric Power, China, 2016 https://kns.cnki.net/KCMS/detail/detail.aspx?dbname=CDFDLAST2017&filename=1016270865.nh.
[37] S.P.X. Chen, Study on CO_2 adsorption performances and kinetics of novel amino solid adsorbents [D], Univ.of Hunan, China, 2021 https://doi.org/10.27135/d.cnki.ghudu.2021.004071.
[38] M. Wickenheisser, F. Jeremias, S.K. Henninger, C. Janiak, Grafting of hydrophilic ethylene glycols or ethylenediamine on coordinatively unsaturated metal sites in MIL-100(Cr) for improved water adsorption characteristics, Inorg. Chim. Acta 407 (2013) 145–152, https://doi.org/10.1016/j.ica.2013.07.024.
[39] Y.H. Miao, Z.J. He, X.C. Zhu, D. Izikowitz, J. Li, Operating temperatures affect direct air capture of CO_2 in polyamine-loaded mesoporous silica, Chem. Eng. J. 426 (2021), 131875, https://doi.org/10.1016/j.cej.2021.131875.
[40] Y. Kuwahara, D.Y. Kang, J.R. Copeland, P. Bollini, C. Sievers, T. Kamegawa, H. Yamashita, C.W. Jones, Enhanced co_2 adsorption over polymeric amines supported on heteroatom-incorporated sba-15 silica: impact of heteroatom type and loading on sorbent structure and adsorption performance, CHEM.-A EUROPEAN J. 18 (52) (2012) 16649–16664, https://doi.org/10.1002/chem.201203144.
[41] C.l. hou., Synthesis of Quaternary Ammonium Functionalized Polymers and Their Application in Direct Air Capture: [D], Univ.of Zhejiang, China, 2021.